Biophysical Model of the Spatial Heterogeneity of Myocardial Flow

Yunlong Huo,[†] Benjamin Kaimovitz,[‡] Yoram Lanir,[‡] Thomas Wischgoll,[§] Julien I. E. Hoffman,[¶] and Ghassan S. Kassab[†*]

[†]Department of Biomedical Engineering, Surgery, and Cellular and Integrative Physiology, Indiana University-Purdue University Indianapolis, Indianapolis, Indiana; [‡]Department of Biomedical Engineering, Israel Institute of Technology, Haifa, Israel; [§]Department of Computer Science and Engineering, Wright State University, Dayton, Ohio; and [¶]Cardiovascular Research Institute, University of California, San Francisco, California

ABSTRACT The blood flow in the myocardium has significant spatial heterogeneity. The objective of this study was to develop a biophysical model based on detailed anatomical data to determine the heterogeneity of regional myocardial flow during diastole. The model predictions were compared with experimental measurements in a diastolic porcine heart in the absence of vessel tone using nonradioactive fluorescent microsphere measurements. The results from the model and experimental measurements showed good agreement. The relative flow dispersion in the arrested, vasodilated heart was found to be 44% and 48% numerically and experimentally, respectively. Furthermore, the flow dispersion was found to have fractal characteristics with fractal dimensions (*D*) of 1.25 and 1.27 predicted by the model and validated by the experiments, respectively. This validated three-dimensional model of normal diastolic heart will play an important role in elucidating the spatial heterogeneity of coronary blood flow, and serve as a foundation for understanding the interplay between cardiac mechanics and coronary hemodynamics.

INTRODUCTION

It is widely acknowledged that the distribution of myocardial blood flow is heterogeneous in small regions of the myocardium (1–11). However, it is difficult to measure the heterogeneity of myocardial blood flow in vivo. Computer simulations and mathematical models can play an important role since experimental approaches to this problem are highly limited, particularly deep in the heart wall. The heterogeneity of myocardial blood flow is affected by many physical factors, such as the architecture of the coronary vasculature, duration of systole, internal and external chamber pressures, regional stresses and strains in the contracting myocardium, vasoactivity of microvasculature, and so on (12). To understand the many factors involved, it is necessary to adapt a staged model approach that gradually considers the various factors and hence increases the degree of realism. The objective of this study was to develop the first stage of such a model, based on three-dimensional (3D) coronary arterial architecture in an arrested heart in the absence of vessel tone. The mathematical, anatomically based analysis of spatial flow heterogeneity was validated with microsphere flow measurements.

We previously analyzed coronary blood flow with the use of an anatomically based coronary arterial tree model (13,14) to understand the longitudinal pressure-flow distribution (15–20). Both steady-state and pulsatile flows were determined based on the entire coronary arterial tree model. Although the model was based on detailed morphometric data (21), it lacked the 3D spatial geometry of the vasculature. Anatomical models with 3D geometrical structure were previously developed by Beard and Bassingthwaighte (22) for the entire coronary arterial tree in a cylindrical model of the heart, and for the first six generations of arteries by Smith et al. (23) in a finite-element model of the heart. Both of these models were based on the morphometric data of Kassab et al. (21). We recently reconstructed a 3D arterial tree model beyond the first six largest generations to include the entire coronary arterial tree down to the first capillary segments in a realistic geometry of the porcine heart (24).

In the study presented here, we developed an anatomically based biophysical model to determine the heterogeneity of regional myocardial flow. The regional myocardial flow heterogeneity predicted by the model was validated experimentally with the use of nonradioactive fluorescent microsphere measurements. The agreement between theory and experiment was very good. The relative dispersion (RD) in the arrested heart was found to be much larger than that in beating hearts, but slightly smaller than that in beating hearts without vascular tone. Furthermore, the RD in any of the three layers examined (i.e., the subepicardium, midwall, and subendocardium) was larger than that of the entire heart. The spatial fractal dimension remained similar in arrested and beating hearts. The physiological implications and limitations of this model were explored in relation to the spatial heterogeneity of coronary blood flow.

MATERIALS AND METHODS

Theoretical model

3D anatomical model

A flow simulation was carried out in the 3D right coronary artery (RCA), left anterior descending (LAD) artery, and left circumflex (LCX) artery tree model recently reconstructed by Kaimovitz et al. (24) based on measured

Submitted January 16, 2009, and accepted for publication February 24, 2009.

*Correspondence: gkassab@iupui.edu

Editor: Michael D. Stern.

0006-3495/09/05/4035/9 $2.00

doi: 10.1016/j.bpj.2009.02.047

morphometric data of Kassab et al. (21). To examine the effect of 3D tree reconstruction, five 3D coronary arterial trees were reconstructed randomly. In the stochastic reconstruction, the arterial vessels were randomly selected subject to 1), published constraints on the planar branching geometry (25); 2), avoidance rules aimed at preventing intersections between vessel segments; and 3), constraints to avoid protrusion of the myocardial wall surfaces. The capillaries were randomly selected and arranged in the sheet along the direction of the myocyte bundles. The 3D trees were largely a dichotomously branching structure (the bifurcation and trifurcation frequencies were ~99% and 1%, respectively). The few collaterals in the swine model were neglected in the model.

The 3D tree model was stochastically reconstructed in two phases. Briefly, in the first phase, geometrical constraints were imposed in a rectangular slab geometry. The constraints were compatible with observed features of coronary branches and measured bifurcation geometry. In the second phase, the reconstructed tree was embedded in a more realistic geometric model of the whole heart by transforming it from the rectangular slab configuration into prolate spheroid epicardial surface. The transformation was carried out by least-square minimization of the deformation in segment lengths, as well as their angular characteristics, subject to the constraint of adhering to the spherical surface geometry. The entire large-scale reconstruction process was parallelized using Message Passing Interface and carried out on a Medium Performance Computing cluster system. The reconstructed trees show close resemblance to native coronary vessels, and their morphological statistics are consistent with the measured morphometric data of Kassab et al. (21). The model spanned the entire spatial range of coronary arteries down to the first capillary vessels based on measured vascular geometry (diameter and length) and branching pattern (connectivity and longitudinal position matrices) (21). The vessels of the RCA, LAD, and LCX arterial trees were spatially distributed in the prolate heart geometry.

Flow simulation

After the spatial branching pattern and vascular geometry of the full 3D coronary arterial trees were generated, a flow analysis was performed in a manner similar to that previously described (17,20). Briefly, the governing equations were Poiseuille's equation ($Q_{ij} = \pi/128\,\Delta P_{ij} G_{ij}$) and conservation of mass ($\sum_{i=1}^{m_j} Q_{ij} = 0$), where $\Delta P_{ij} = P_i - P_j$, $G_{ij} = D_{ij}^4/\mu_{ij} L_{ij}$, and D_{ij}, L_{ij}, and μ_{ij} are the diameter, length, and viscosity, respectively, between nodes i and j, and m_j is the number of vessels converging at the jth node. The final global matrix formulation might be written as $\mathbf{GP} = \mathbf{G_B}\,\mathbf{P_B}$, where $\mathbf{G}$ is the matrix of conductance, $\mathbf{P}$ is the column vector of the unknown nodal pressures, and $\mathbf{G_B}\,\mathbf{P_B}$ is the column vector of the conductance times the boundary pressure of their attached vessels. The pressure at the inlet and outlet was set as 100 and 26 mmHg, respectively. The viscosity (μ_{ij}) was selected as 1.1 cp to mimic our cardioplegic solution containing albumin. Furthermore, the viscosity was considered as a function of vessel (26) for blood.

Dividing the 3D model

The prolate left ventricular (LV) model encompassing the 3D coronary arterial tree was numerically divided into small plugs with the same size and spatial distribution as those described below in ''Experimental methods''. Briefly, the hollow truncated ellipsoid was formed by rotating two ellipses about their major axis (z axis). The detailed dimensions of the ellipsoid can be found elsewhere (24). The ellipsoid was first divided into six rings along its major axis (z axis), as shown in Fig. 1 *a*. Each ring was then divided into seven, seven, seven, four, three, and two thick plugs (including the subepicardium, midwall, and subendocardium) rotated around its major axis corresponding to the experimental preparation (see details below). Each thick plug was then divided into the subepicardium, midwall, and subendocardium plugs from the outer to inner surfaces, as shown in Fig. 1 *b*. Each plug was further divided into eight pieces of 0.125 g myocardium, as shown in Fig. 1 *c*, to analyze the fractal nature of predicted regional myocardial blood flow heterogeneity. The regional flow was calculated as the sum of the magnitude of flow through all first segments of the capillary vessels in each plug.

Experimental methods

Animal preparation

Studies were performed on six 3- to 4-month-old farm pigs weighing 28–38 kg. The experimental procedures of the animal preparation were similar to those described by Kassab et al. (21). All animal experiments were performed in accordance with national and local ethics guidelines, including the Institute of Laboratory Animal Research guide, Public Health Service policy, the Animal Welfare Act, and an approved University of California, Irvine, Institutional Animal Care and Use Committee protocol.

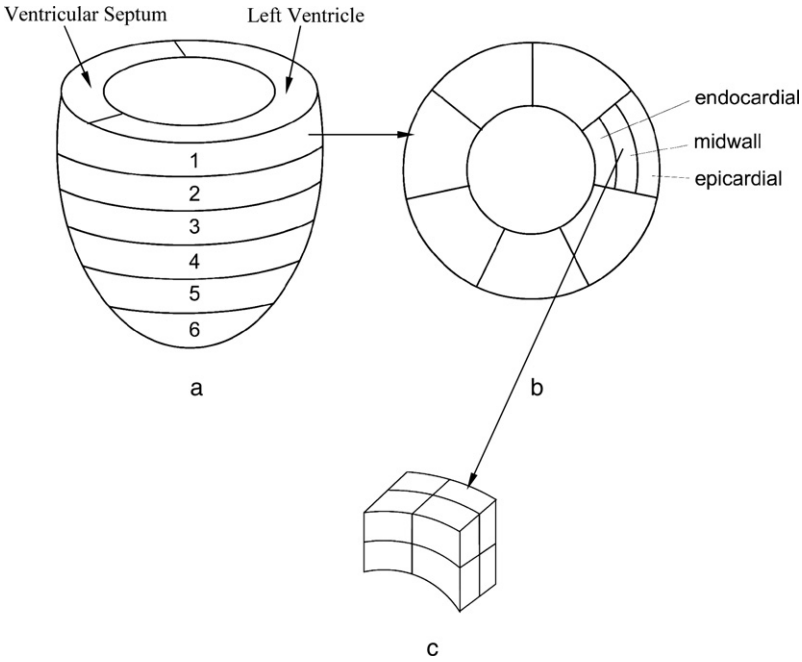

FIGURE 1 Schematic representation of experimental sectioning of the porcine hearts into (*a*) different rings and (*b*) small plugs (subepicardium, midwall, and subendocardium). (*c*) Numerical sectioning of each plug in the 3D model corresponding to experimental sections.

Microsphere injections

After the heart was isolated, it was placed in a cold (0°C) saline bath as shown in Fig. 2. The major coronary arteries (RCA, LAD artery, and LCX artery) were cannulated under saline to avoid air bubbles. For measurement of flow and pressure, the flow transducers (Transonic Systems, Ithaca, NY; relative error of ±2% at full scale) were mounted on the coronary arteries directly and the pressure transducer (Summit Disposable Pressure Transducer, Baxter Healthcare, Deerfield, IL; error of ±2% at full scale) was connected at the inlet of the coronary arteries through a Y tube. A hypothermic (10°C), isotonic, cardioplegic rinsing solution was contained in a 2-L bottle hung above the heart and injected into the coronary arteries. The rinsing solution was composed of 2,3-butanedione monoxime, 1.5 g/L; adenosine, 0.1 g/L; and albumin, 10 g/L, which was found to be effective in maintaining the heart in a relaxed state. In particular, the viscosity (μ) was equal to ~1.1 cp for the cardioplegic solution of 10°C when the heart was placed in a cold (0°C) saline bath. The coronary perfusion pressure was 100 mmHg and the LV pressure was 0 mmHg in the arrested heart. The coronary sinus pressure was zero (vented) and the pressure at each outlet of first segments of arterial capillary was assumed equal to 26 mmHg (19,20).

Regional coronary blood flow was measured with injections of fluorescent microspheres of 15 μm diameter (Molecular Probes, Eugene, OR). The steady-state flow rate was kept constant for ~5–10 min. A minimum of 400 microspheres were needed per tissue piece to ensure 95% confidence that the flow measurement was within 10% of the true value (27). We doubled the minimum number to make sure that low-flow organ pieces also had an adequate number of microspheres. Before injection, the microspheres were agitated and dispersed through vigorous agitation and ultrasonic water bath, respectively. The microspheres were injected into the cannulated coronary arteries with the cardioplegic rinsing solution through Tygon tubing, as shown in Fig. 2. A slow and steady rate of injection was implemented to keep pressure and flow rate constant.

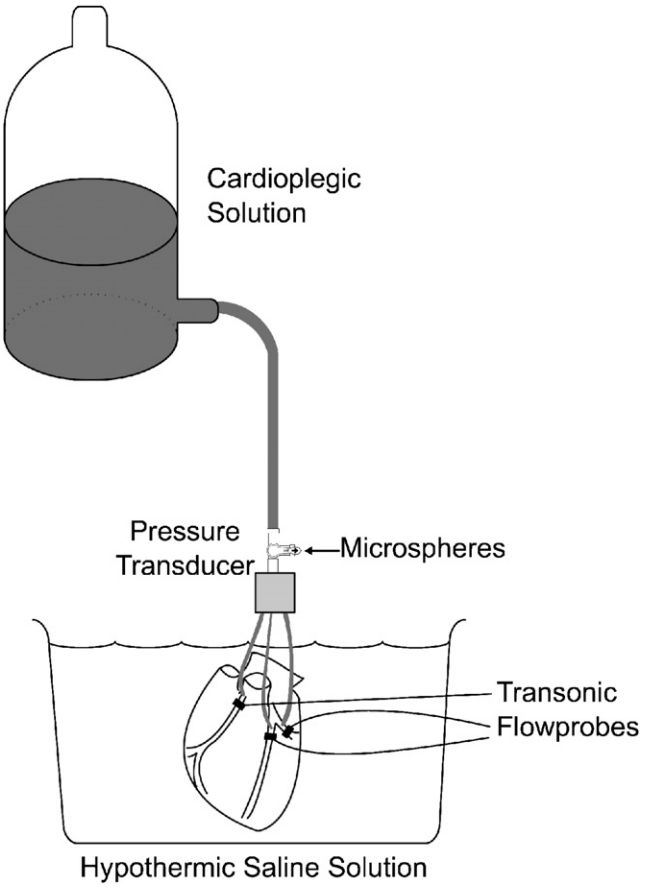

FIGURE 2 Schematic representation of microsphere injection.

Dividing hearts and counting samples

After injection, the atria and the right ventricular (RV) free wall were removed and large epicardial vessels were trimmed off. Subsequently, the heart was divided perpendicularly to the long axis into six rings as illustrated in Fig. 1, *a* and *b*. The rings of the LV and ventricular septum were frozen to stiffen the muscle to facilitate subsequent sectioning. Different rings were then divided radially into different sectors as seven, seven, seven, four, three, and two pieces from top to bottom, respectively (labeled as 1–6 in Fig. 1 *a*, respectively). Each sector was sliced into three plugs (subepicardium, midwall, and subendocardium), as shown in Fig. 1 *b*. Each plug was weighed immediately after slicing and their weights ranged from 0.74 to 1.19 g with a mean value of ~1 g. There were ~90 plugs per LV and septum (the weight of the LV and septum was ~90 g). The adjacent pieces of plugs were assembled to form large plugs (e.g., plugs of 2, 4, 6, and 8 g). The assembled adjacent plugs were then carefully weighed to construct plugs of a more uniform large size.

After sectioning, the tissue (each plug) was digested with KOH and the microspheres were physically separated from the tissue by negative pressure filtration. The microspheres were finally measured in a spectrometer (LS 55; Perkin Elmer). The detailed procedure for the measurement of microspheres can be found in the standard manual from Fluorescent Microsphere Resource Center.

Data analysis

The analysis of the heterogeneity of regional blood flow was carried out as described by Bassingthwaighte et al. (3–8). The F-test and two-sample *t*-test were used to compare relative regional flows between the experiment and the 3D model. The Pearson product moment correlation coefficient was adopted to analyze flows in different layers (subepicardium, midwall, and subendocardium).

RESULTS

Validation of the 3D model

The flow and pressure were calculated in each of five reconstructions. Fig. 3 *a* shows the mean ± SD; both the mean pressure and mean flow over each order are averaged in five reconstructions) for the pressure-flow relationship of blood in five reconstructions of 3D tree models, which were found to be mutually very similar (small SD). The mean inlet flow and equivalent resistance for the five simulations of the LCX arterial tree were 0.44 ± 0.02 (mL/s) and 167 ± 9 (mmHg · s/mL) for blood, respectively, and 1.27 ± 0.05 (mL/s) and 58 ± 4 (mmHg · s/mL) for cardioplegic solution. The experimentally measured flow at the inlet of the LCX artery, as shown in Fig. 2, was 1.16 ± 0.12 (mL/s) for cardioplegic solution, which agreed reasonably with the numerical result. Although the different tree reconstructions led to regional variation of blood flow in the LV and septum, the relative flow dispersion and fractal dimension were very similar. Since the variations within a single simulation were significantly larger than variations between simulations, a typical anatomical reconstruction was used to simulate flow and pressure distributions.

The 3D model was also compared with a previously published model that did not consider the 3D spatial geometry (20) to validate the pressures and flows. Fig. 3 *b* shows the

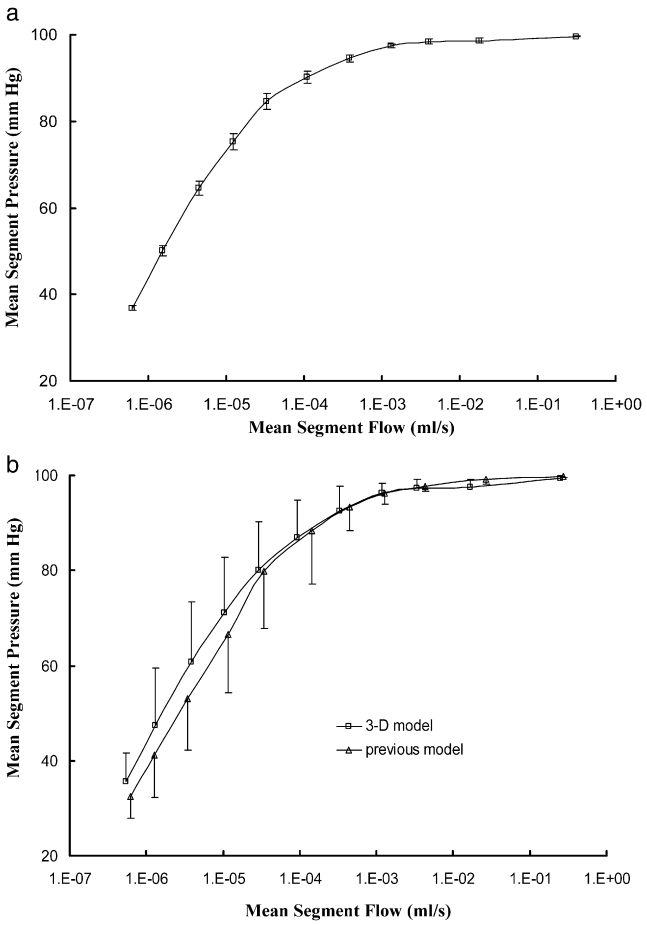

FIGURE 3 (*a*) Mean ± 1 SD for pressure-flow relationship of blood in five reconstructions of 3D models (both mean pressure and mean flows over each order are averaged over five reconstructions). (*b*) Comparison of pressure-flow relationships of blood using the LCX in one representative 3D model and a previous LCX arterial tree model (20) (the pressure and flow are averaged for each order of the arterial tree models).

relationship between mean flow and mean pressure ±1 SD (average for each order) of blood for the LCX in the 3D model and a previously published LCX arterial tree (20). Fig. 3 *b* depicts similar computational results, and the 3D

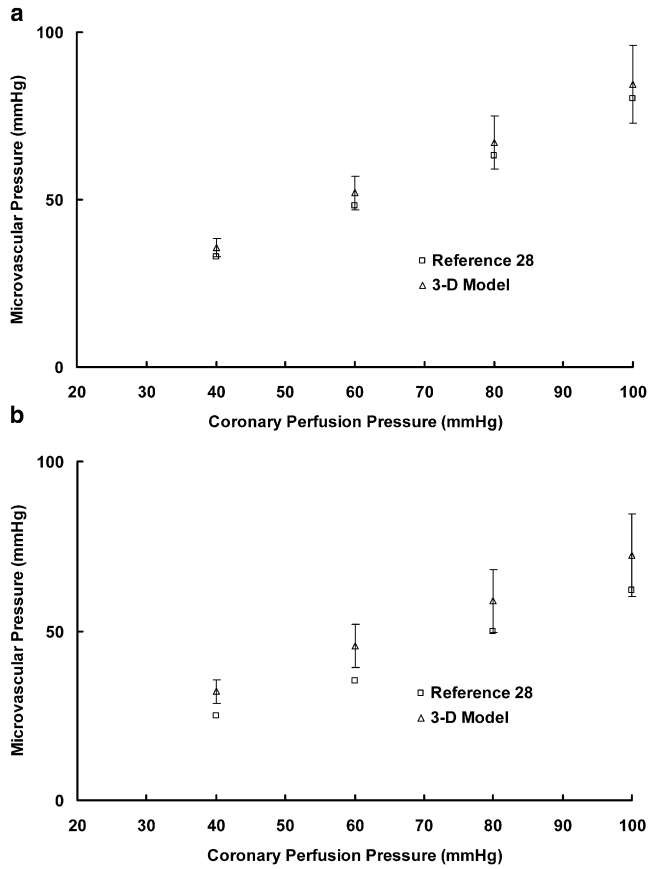

FIGURE 5 Arteriolar pressures in the (*a*) subepicardial and (*b*) subendocardial microcirculation at orders 5 and 6 (with vessel diameter range of 64.4–150 μm) of the LAD arterial tree at different coronary perfusion pressures, which agree reasonably well with the data of Chilian (28).

model agrees well with the previous mathematical model (within 1 SD of the 3D model). Fig. 4 illustrates the pressure distribution in two views (lateral left and posterolateral oblique left) of the entire coronary arterial tree model down to the first capillary segments. It is clear that the pressure distribution is fairly uniform in larger vessels and changes significantly in smaller vessels (<100 μm). Fig. 5, *a* and *b*, show the arteriolar pressures in the subepicardial

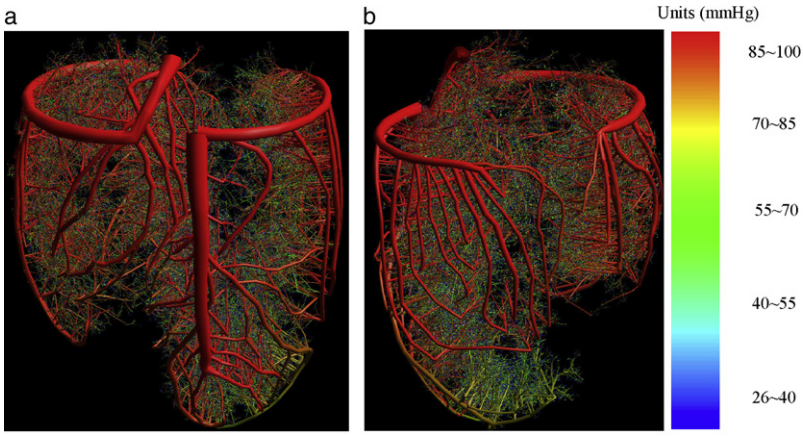

FIGURE 4 Pressure distribution in two views (lateral left and posterolateral oblique left) in the 3D entire coronary arterial trees consisting of the epicardial, transmural, and perfusion subnetworks: (*a*) lateral-left-view pressure and (*b*) posterolateral-oblique-left-view pressure.

and subendocardial microcirculation at orders 5 and 6 (with vessel diameter in the range of 64.4–150 μm) of the LAD arterial tree, respectively, at different coronary perfusion pressures, which agree with the data of Chilian (28).

Fractal nature of flow heterogeneity

The 3D coronary arterial model presented here provides a platform to analyze the distribution and heterogeneity in small neighboring regions of the myocardium. To be consistent with experimental measurements, all numerical results were calculated for cardioplegic solution with a viscosity (μ) of 1.1 cp. Table 1 shows a statistical comparison of the regional flow between the model and the ex vivo experiment in Fig. 2. Table 1 (*A*) shows the results of the F-test for relative regional flows between the experiment and the 3D model ($p > 0.99$ when a two-sample *t*-test was used). The F-test (a value of unity implies the same dispersion) is used to test whether the SDs of two populations (i.e., experimental and numerical regional flows in this study) are equal. As shown in Table 1 (*A*), the variances of the relative regional flows between experimental and numerical results are not statistically different. From the 3D model for cardioplegic solution, myocardial flows were calculated as 2.04, 2.84, and 2.29 mL/min/g in the subepicardium, midwall, and subendocardium, respectively, which is similar to the experimental measurement with values of 1.95, 2.32, and 2.24 mL/min/g, respectively. Myocardial flows averaged over the entire myocardial wall were 2.39 and 2.17 mL/min/g in the heart in the 3D model and microsphere measurements, respectively, which corresponds to 359 and 326 mL/min in a heart of 150 g. Table 1 (*B*) shows a radial or transmural comparison of myocardial flows in different layers. The numerical correlations in adjacent layers (subepicardium or subendocardium versus midwall) are larger than in nonadjacent layers (subepicardium versus subendocardium), which is consistent with experimental observations. The numerical and experimental results show similar ratios of mean flows in different layers. Table 2 lists the RDs of the spatial distribution of flows in three transmural layers. The numerical results agree very well with the experimental data.

TABLE 1

Animal No.	F-value, 3D model versus experiments	Degrees of freedom in 3D model vs. experiments
1	0.59	90: 72
2	0.98	90: 84
3	0.84	90: 101
4	0.47	90: 86
5	0.50	90: 72
6	0.79	90: 73

(*A*)

Animal No.	R^2 (square of Pearson product moment correlation coefficient)			Inner: Middle: Outer (ratio of mean flows in subendocardium, midwall, and subepicardium)
	Outer versus Middle	Middle versus Inner	Outer versus Inner	
1	0.55	0.84	0.48	1.05: 1.27: 1
2	0.78	0.86	0.71	0.95: 1.11: 1
3	0.81	0.88	0.71	1.05: 1.02: 1
4	0.88	0.90	0.79	1.16: 1.22: 1
5	0.93	0.94	0.88	1.60: 1.51: 1
6	0.63	0.68	0.6	1.09: 1.00: 1
Mean	0.76	0.85	0.69	1.15: 1.19: 1
3D model	0.72	0.83	0.48	1.12: 1.39: 1

(*B*)

(*A*) F-test for the relative regional flow (3) (the mean value of plugs is ~1 g) between experiments and the 3D model ($p > 0.99$ when a two-sample *t*-test is implemented). (*B*) Comparison of flow in radially corresponding regions from different layers (outer, subepicardium; middle, midwall; inner, subendocardium).

TABLE 2 RD in each layer (subepicardium, midwall, and subendocardium) in ex vivo experiments and the 3D model

Animal No.	Relative flow dispersion in LV and septum, %			
	Subepicardium	Midwall	Subendocardium	Global
1	51	27	35	44
2	50	40	45	45
3	52	47	52	50
4	46	48	52	55
5	37	41	58	46
6	53	42	34	47
Mean $\pm$ SD	48 $\pm$ 6	41 $\pm$ 7.5	46 $\pm$ 10	47.8 $\pm$ 4
3D model	47	42	53	44

Degree of heterogeneity can be expressed by the RD (RD = SD/mean) of the values of f_i, where f_i is the relative regional flow in the region (3).

Bassingthwaighte et al. (3–8) indicated that fractal phenomena describe regional flows within the heart, skeletal muscle, and other organs. In their studies, they showed that a simple fractal relation provides precise descriptions of the heterogeneity of regional and myocardial blood flows over a wide range of piece sizes. Here, we used our 3D coronary arterial trees to simulate the spatial flow distribution in the LV and septum of porcine hearts and investigated the fractal nature of regional myocardial blood flow heterogeneity in diastole in the absence of vessel tone. Two methods for fractal analysis were implemented: one (the fractal regression) relating to the effect of plug size on flow dispersion, and one (correlation versus interval relationship) relating to the effect of distance between plugs on the correlation between their flows. Fig. 6 *a* shows the fractal regression for spatial flow in the LV and septum. A power curve fit reveals a fractal dimension, *D*, with a value of 1.25 ($R^2 = 0.98$) and 1.27 ($R^2 = 0.99$) for the computational model and experimental data (microsphere measurements in six porcine hearts), respectively. Furthermore, Fig. 6 *b* shows the fractal regression for spatial flow in three layers of the LV and septum (subepicardium, midwall, and subendocardium) obtained from experiments (mean $\pm$ 1 SD) and the 3D model. The solid, dashed, and dotted lines represent the results of the 3D model for the subendocardium, midwall, and subepicardium, respectively. A power fit for fractal regression in the 3D model shows exponents of 1.45 ($R^2 = 0.99$), 1.46 ($R^2 = 0.98$), and

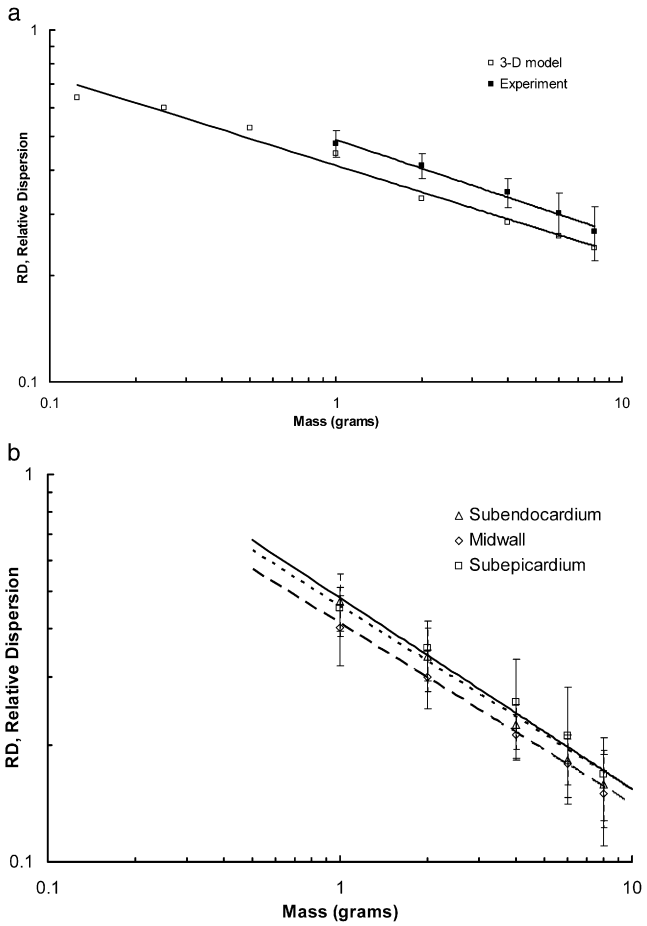

FIGURE 6 (*a*) Fractal regression for spatial flow in the LV and septum myocardium. The fractal nature can be represented as $\mathrm{RD}(m) = \mathrm{RD}(m_{\mathrm{ref}}) \cdot [m/m_{\mathrm{ref}}]^{1-D}$ (3), where m is the mass of the pieces of tissue in grams, D is the spatial fractal dimension, and the reference level of dispersion, $\mathrm{RD}(m_{\mathrm{ref}})$, is taken arbitrarily to be the RD found using pieces of mass m_{ref}, which is chosen to be 1 g. Through the power curve fits of fractal regression, the exponent has values of 1.25 ($R^2 = 0.98$) and 1.27 ($R^2 = 0.99$) for the computational results (3D model) and experimental results (microsphere measurements in six pig hearts), respectively. (*b*) The fractal regression for spatial flow in three layers of the LV and septum (subepicardium, midwall, and subendocardium) obtained from experiments (mean ± 1 SD) and the 3D model. The solid, dashed, and dotted lines represent the results of the 3D model for the subendocardium, midwall, and subepicardium, respectively. A power fit for fractal regression in the 3D model shows exponents of 1.47 ($R^2 = 0.99$), 1.47 ($R^2 = 0.98$), and 1.49 ($R^2 = 0.98$) for the subepicardium, midwall, and subendocardium, respectively. These agree well with the experimental values (six hearts) of 1.47, 1.45, 1.51 for the subepicardium, midwall, and subendocardium, respectively.

1.48 ($R^2 = 0.98$) for the subepicardium, midwall, and subendocardium, respectively. These agree well with the experimental values (six hearts) of 1.47, 1.45, and 1.51 for the subepicardium, midwall, and subendocardium, respectively. Finally, Fig. 7 shows the relationship between the correlation coefficient, r_n, and the number of separating intervals, n, at three different levels of spatial resolution (three from the model and one from the microsphere measurements). Here, the solid and dashed lines represent the Hurst coefficient of

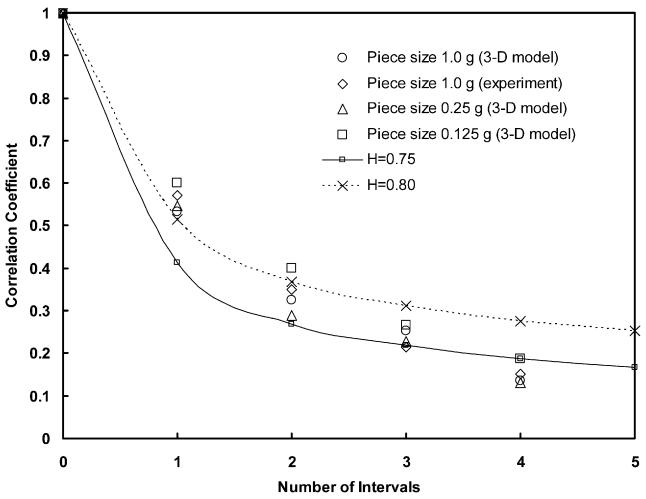

FIGURE 7 Effect of interplug distance on the correlation between plug flows, expressed as the relationship between the correlation coefficient, r_n, and the number of interplug intervals, n, at three different levels of spatial resolution (three from model and one from microsphere measurement). The correlation coefficients between pieces centered n units apart, r_n, can be calculated as: $r_n = 1/2[(n-1)^{2H} - 2n^{2H} + (n+1)^{2H}]$, where H is the Hurst coefficient (42,6). The relationship between the Hurst coefficient and the spatial fractal dimension can be represented by the equation ($H = 2 - D$). Here the solid and dashed lines represent Hurst coefficients of 0.75 and 0.8, respectively.

0.75 and 0.80, respectively. Since the fractal dimension, D, can be represented by the equation ($D = 2 - H$), it has the same value (1.25, 1.20) as the prediction by the 3D model when H is equal to 0.75 and 0.80, respectively.

DISCUSSION

To our knowledge, this is the first study to predict coronary flow heterogeneity based on a mathematical model comprised of the 3D coronary arterial tree in the myocardium. Predictions of the flow heterogeneity of the mathematical model were validated by experimental measurements using fluorescent microspheres. The fractal nature of flow heterogeneity was predicted by the model and confirmed by the experiments. The results and their implications are discussed below.

Pressure-flow relation

The longitudinal pressure distributions are depicted in Figs. 3 and 4. The 3D reconstruction algorithm presented here is based on anatomical and physiological observations (25,29,30), and thus is clearly different from the previous two-step growth algorithm (13). The pressure-flow (Fig. 3 *b*) relations were similar for the 3D model and previous two-step models, although a relatively large difference occurred at the low order levels in Fig. 3 *b* because of a larger number of vessels in the 3D reconstruction algorithms. The quantitative (Fig. 3, *a* and *b*) and visual results (Fig. 4) clearly illustrate a uniform pressure in the larger arteries and a significant drop in pressure for

vessels <100 μm in diameter, which is in agreement with experimental measurements (28,31,32). The arteriolar pressures (Fig. 5, *a* and *b*) were found to be higher at the epicardial as compared with the subendocardial surfaces for each respective order, which is consistent with experimental observations (28). A slight difference in the subendocardium with pressures of 40 and 60 mmHg may be due to the larger size of the pigs used in this study (28–38 kg, which is 2–3 times larger than the pigs used by Chilian (28) (7–15 kg).

Flow heterogeneity

The heterogeneous myocardial flows were analyzed both numerically and experimentally. The statistical analysis in Table 1 (*A*) shows that the variances of the relative regional flows obtained from the 3D model are not significantly different from the experimental measurements. Our numerical and experimental studies (Table 1 (*B*)) show that there is a stronger correlation in adjacent layers than in nonadjacent layers, which is consistent with a previous experimental observation in arrested dog hearts without vascular tone (2). Furthermore, we report that the mean flow in the midwall and subendocardium is higher than that in the subepicardium, as previously determined in arrested porcine hearts (28).

There are small differences in mean blood flow between the subepicardial and subendocardial layers of the normal heart (33,34), whereas flows are higher in subendocardial than in subepicardial layers in maximally dilated hearts (35). The RD in the arrested hearts, as shown in Table 2, is larger than that in normal physiological condition (3), but smaller than that in beating hearts without vascular tone (2). This illustrates that the vascular tone has a significant effect on the heterogeneity of myocardial flows. The vascular tone is determined by many different competing vasoconstrictor and vasodilator factors acting on the blood vessel, and plays a critical role in regulating pressure and flow. It affects the flows and pressures distal to the site of resistance (36), leading to more uniform regional blood flow, and has smaller heterogeneity in the in vivo state. The heterogeneity in beating hearts without vascular tone is affected mainly by mechanical factors such as myocardial workload, metabolic rate, etc. The most important effect may be the heterogeneity of local work and local ATP hydrolysis for contraction (8), which is associated with oxygen consumption. Prinzen et al. (37,38) found that early activation leads to only small shortening strain during ejection, and late activation leads to large ejection phase shortening. Rapid shortening against low resistance reduces ATP hydrolysis because of shortening deactivation (39,40). These mechanical factors during the isovolumetric phase of systole may increase the heterogeneity in beating hearts without vascular tone in comparison with the arrested heart.

The RD in the 3D model (Table 2 and Fig. 6 *a*) was smaller than the experimental measurements but still within $\pm$ 1 SD. Of interest, the within-layer (subepicardium, midwall, and subendocardium) RD showed better agreement between theory and experiment. Both numerical and experimental results show that the spatial fractal dimension D (Fig. 6 *b*) is larger in the three layers than in the entire LV and septum. This implies that the within-layer randomness is stronger than that of the entire thickness, which illustrates the role of correlation of radial flow.

Fractal flows

The fractal nature of regional myocardial blood flow heterogeneity can be simulated in the 3D model. As described by Bassingthwaighte et al. (3), the fractal nature implies that the variation in regional flow can be described with two parameters, RD(m_{ref}) and the slope of the logarithmic relationship defined by the spatial fractal dimension D. At present, D (Fig. 6 *a*) has values of 1.25 and 1.27 determined by least-square power curve fits of data obtained from the 3D coronary arterial tree model and microsphere measurement, respectively. The present computed fractal dimension is slightly larger than the value of 1.23 reported by Bassingthwaighte et al. (3).

The Hurst coefficient, $H = 2 - D$, was further used to analyze the dispersion independently of the myocardial size. The results from the 3D model and microsphere measurement relating to the correlation coefficient, r_n, show similar trends (Fig. 7). The Hurst coefficient, H, with values of 0.75 and 0.80 agreed better with the experimental and numerical results on the nearest-neighbor correlations at 3 and 4 intervals and at 1 and 2 intervals, respectively. This implies that the spatial fractal dimension, D, is in the range of 1.20–1.25. Using various statistical methods in this study, we obtained results similar to those of Bassingthwaighte et al. (3). In agreement with reports by Glenny (41) and Beard and Bassingthwaighte (22), the correlation coefficient, r_5, was found to fall below the curve and may possibly be negative.

Critique of the study

Although our 3D model is based on detailed measured morphometric data from coronary vessels, a few assumptions remain: 1), the venous system is decoupled from the arterial tree; 2), the steady-state flow is calculated instead of more realistic pulsatile flow; and 3), the effects of other physiological and mechanical factors are ignored. In future studies, the arterial circuit will be extended to the entire coronary vasculature, i.e., we will connect the functional capillaries to the entire venous system. Hence, we will include the coronary venous pressure as the outlet boundary condition. In addition, the effect of flow pulsatility will be calculated in the entire 3D coronary model associated with the myocardial/vascular interaction in systole, and various physiological and mechanical factors will also be included to advance the current 3D model.

The pressure boundary condition at the outlet of the first capillary segments was taken to be uniform (ad hoc assumption of 26 mmHg). We previously showed that dispersion of

pressure at the capillary level will increase the coefficient of variance of capillary flow (20). Hence, the RD in the 3D model may be an underestimation of the reality of arrested hearts given the assumption of zero dispersion of capillary pressure. This may partly explain the smaller RD obtained by the 3D model as compared with the ex vivo experimental data (Table 2 and Fig. 6 *a*). An additional explanation may be the lack of a venous system in the 3D model, in contrast to the physical heart.

Significance of the study

This study presents a mathematical model to predict the spatial heterogeneity of myocardial flow. The proposed model makes use of physical and mathematical principles, with the help of anatomical and experimental measurements, to explain and predict some aspects of spatial flow distribution of the coronary arterial circulation in quantitative terms. The 3D model is found to be in good agreement with the experimental data. The validated 3D model of normal diastolic hearts will serve as a physiological reference state that can be used to investigate drug delivery and metabolic exchange among many other issues. This 3D model will also serve to quantitatively test various hypotheses regarding the spatial distribution of flow in the coronary circulation.

We thank Carlos Linares for excellent technical assistance.

This research was supported in part by the U.S.-Israel Binational Science Foundation (grant 2003-095); the National Heart, Lung, and Blood Institute, National Institutes of Health (grants HL084529 and HL087235); and an American Heart Association Scientist Development Grant (0830181N).

REFERENCES

1. Austin, R. E., G. S. Aldea, D. L. Coggins, A. E. Flynn, and J. I. E. Hoffman. 1990. Profound spatial heterogeneity of coronary reserve: discordance between patterns of resting and maximal myocardial blood flow. *Circ. Res.* 67:319–331.
2. Austin, Jr., R. E., N. G. Smedira, T. M. Squiers, and J. I. Hoffman. 1994. Influence of cardiac contraction and coronary vasomotor tone on regional myocardial blood flow. *Am. J. Physiol. Heart Circ. Physiol.* 266:H2542–H2553.
3. Bassingthwaighte, J. B., R. B. King, and S. A. Roger. 1989. Fractal nature of regional myocardial blood flow heterogeneity. *Circ. Res.* 65:578–590.
4. Bassingthwaighte, J. B., M. A. Malone, T. C. Moffett, R. B. King, I. S. Chan, et al. 1990. Molecular and particulate depositions for regional myocardial flows in sheep. *Circ. Res.* 66:1328–1344.
5. Bassingthwaighte, J. B., M. A. Malone, T. C. Moffett, R. B. King, S. E. Little, et al. 1987. Validity of microsphere depositions for regional myocardial flows. *Am. J. Physiol. Heart Circ. Physiol.* 253:H184–H193.
6. Bassingthwaighte, J. B., and R. P. Beyer. 1991. Fractal correlation in heterogeneous systems. *Physica D.* 53:71–84.
7. Bassingthwaighte, J. B., and D. A. Beard. 1995. Fractal ^{15}O-water washout from the heart. *Circ. Res.* 77:1212–1221.
8. Bassingthwaighte, J. B., D. A. Beard, and Z. Li. 2001. The mechanical and metabolic basis of myocardial blood flow heterogeneity. *Basic Res. Cardiol.* 96:582–594.
9. King, R. B., J. B. Bassingthwaighte, J. R. Hales, and L. B. Rowell. 1985. Stability of heterogeneity of myocardial blood flow in normal awake baboons. *Circ. Res.* 57:285–295.
10. Mori, H., M. Chujo, S. Haruyama, H. Sakamoto, Y. Shinozaki, et al. 1995. Local continuity of myocardial blood flow studied by monochromatic synchrotron radiation–excited x-ray fluorescence spectrometry. *Circ. Res.* 76:1088–1100.
11. Stapleton, D., J. van Beek, S. A. Roger, D. G. Baskin, and J. B. Bassingthwaighte. 1988. Regional myocardial flow heterogeneity assessed with 2-iododesmethylimipramine. *Circulation.* 78 (Suppl. II):405.
12. Hoffman, J. I. E., and J. A. E. Spaan. 1990. Pressure-flow relations in coronary circulation. *Physiol. Rev.* 70:331–390.
13. Mittal, N., Y. Zhou, S. Ung, C. Linares, S. Molloi, et al. 2005. A computer reconstruction of the entire coronary arterial tree based on detailed morphometric data. *Ann. Biomed. Eng.* 33:1015–1026.
14. Wischgoll, T., J. S. Choy, E. L. Ritman, and G. S. Kassab. 2008. Validation of image-based method for extraction of coronary morphometry. *Ann. Biomed. Eng.* 36:356–368.
15. Huo, Y., and G. S. Kassab. 2006. Pulsatile blood flow in the entire coronary arterial tree: theory and experiment. *Am. J. Physiol. Heart Circ. Physiol.* 291:H1074–H1087.
16. Huo, Y., and G. S. Kassab. 2007. A hybrid one-dimensional/Womersley model of pulsatile blood flow in the entire coronary arterial tree. *Am. J. Physiol. Heart Circ. Physiol.* 292:H2623–H2633.
17. Huo, Y., C. Linares, and G. S. Kassab. 2007. Capillary perfusion and wall shear stress are restored in the coronary circulation of hypertrophic right ventricle. *Circ. Res.* 100:273–283.
18. Huo, Y., and G. S. Kassab. 2009. Scaling of blood flow resistance: from single vessel to entire distal tree. *Biophys. J.* 96:339–346.
19. Kassab, G. S., J. Berkley, and Y. C. Fung. 1997. Analysis of pig's coronary arterial blood flow with detailed anatomical data. *Ann. Biomed. Eng.* 25:204–217.
20. Mittal, N., Y. Zhou, C. Linares, S. Ung, B. Kaimovitz, et al. 2005. Analysis of blood flow in the entire coronary arterial tree. *Am. J. Physiol. Heart Circ. Physiol.* 289:H439–H446.
21. Kassab, G. S., C. A. Rider, N. J. Tang, and Y. C. Fung. 1993. Morphometry of pig coronary arterial trees. *Am. J. Physiol. Heart Circ. Physiol.* 265:H350–H365.
22. Beard, D. A., and J. B. Bassingthwaighte. 2000. The fractal nature of myocardial blood flow emerges from a whole-organ model of arterial work. *J. Vasc. Res.* 37:282–296.
23. Smith, N. P., A. J. Pullan, and P. J. Hunter. 2000. The generation of an anatomically accurate geometric coronary geometric coronary model. *Ann. Biomed. Eng.* 28:14–25.
24. Kaimovitz, B., Y. Lanir, and G. S. Kassab. 2005. Large-scale 3-D geometric reconstruction of the porcine coronary arterial vasculature based on detailed anatomical data. *Ann. Biomed. Eng.* 33:1517–1535.
25. Zamir, M. 1978. Nonsymmetrical bifurcations in arterial branching. *J. Gen. Physiol.* 72:837–845.
26. Pries, A. R., D. Neuhaus, and P. Gaehtgens. 1992. Blood viscosity in tube flow: dependence on diameter and hematocrit. *Am. J. Physiol. Heart Circ. Physiol.* 163:H1770–H1778.
27. Buckberg, G. D., J. C. Luck, D. B. Payne, J. I. E. Hoffman, J. P. Archie, et al. 1971. Some sources of error in measuring regional blood flow with radioactive microspheres. *J. Appl. Physiol.* 31:598–604.
28. Chilian, W. M. 1991. Microvascular pressures and resistances in the left ventricular subepicardium and subendocardium. *Circ. Res.* 69:561–570.
29. Murray, C. D. 1926. The physiological principle of minimum work applied to the angle of branching of arteries. *J. Gen. Physiol.* 9:835–841.
30. Van Bavel, E., and J. A. Spaan. 1992. Branching patterns in the porcine coronary arterial tree: estimation of flow heterogeneity. *Circ. Res.* 71:1200–1212.
31. Chilian, W. M., S. M. Layne, E. C. Klausner, C. L. Eastham, and M. L. Marcus. 1989. Redistribution of coronary microvascular resistance produced by dipyridamole. *Am. J. Physiol. Heart Circ. Physiol.* 256:H383–H390.
32. Kanatsuka, H., K. G. Lamping, C. L. Eastham, M. L. Marcus, and K. C. Dellsperger. 1991. Coronary microvascular resistance in hypertensive cats. *Circ. Res.* 68:726–733.

33. Hofman, M. B., A. C. van Rossum, M. Sprenger, and N. Westerhof. 1996. Assessment of flow in the right human coronary artery by magnetic resonance phase contrast velocity measurement: effects of cardiac and respiratory motion. *Magn. Reson. Med.* 35:521–532.

34. Klocke, F. J., R. E. Mates, J. M. Canty, Jr., and A. J. Ellis. 1985. Coronary pressure-flow relationships. Controversial issues and probable implications. *Circ. Res.* 56:310–323.

35. Verrier, E. D., R. W. Baer, R. F. Hickey, G. J. Vlahakes, and J. I. E. Hoffman. 1982. Transmural pressure-flow relations during diastole in the canine left ventricle. *Circulation.* 62 (Suppl. III):62 (Abstr.)

36. Intaglietta, M. 1981. Vasomotor activity, time-dependent fluid exchange and tissue pressure. *Microvasc. Res.* 21:153–164.

37. Prinzen, F. W., C. H. Augustijn, T. Arts, M. A. Allessie, and R. S. Reneman. 1990. Redistribution of myocardial fiber strain and blood flow by asynchronous activation. *Am. J. Physiol. Heart Circ. Physiol.* 259:H300–H308.

38. Prinzen, F. W., C. H. Augustijn, M. A. Allessie, T. Arts, T. Delhaas, et al. 1992. The time sequence of electrical and mechanical activation during spontaneous beating and ectopic stimulation. *Eur. Heart J.* 13:535–543.

39. Landesberg, A., and S. Sideman. 1994. Mechanical regulation of cardiac muscle by coupling calcium kinetics with cross-bridge cycling: a dynamics model. *Am. J. Physiol. Heart Circ. Physiol.* 267:H779–H795.

40. Landesberg, A., and S. Sideman. 1994. Coupling calcium binding to troponin C and cross-bridge cycling in skinned cardiac cells. *Am. J. Physiol. Heart Circ. Physiol.* 266:H1260–H1271.

41. Glenny, R. W. 1992. Spatial correlation of regional pulmonary perfusion. *J. Appl. Physiol.* 72:2378–2386.

42. Van Beek, J. H., S. A. Roger, and J. B. Bassingthwaighte. 1989. Regional myocardial flow heterogeneity explained with fractal networks. *Am. J. Physiol. Heart Circ. Physiol.* 257:H1670–H1680.